Ultra-High Resolution ^{17}O Solid-State NMR Spectroscopy of Biomolecules: A Comprehensive Spectral Analysis of Monosodium L-Glutamate·Monohydrate

Alan Wong,[†,φ,*] Andy P. Howes,[†] Jonathan R. Yates,[‡] Anthony Watts,[§] Tiit Anupõld,[¶] Jaan Past,[¶] Ago Samoson,[¶,†] Ray Dupree,[†,*] Mark E. Smith[†,*]

[†]Department of Physics, University of Warwick, Coventry, CV4 7AL, United Kingdom

[φ]CEA Saclay, DSM, IRAMIS, UMR CEA/CNRS no 3299 – SIS2M, Laboratoire Structure et Dynamique par Résonance Magnétique, F-91191, Gif-sur-Yvette Cedex, France

[‡]University of Oxford, Department of Materials, Parks Road, Oxford, OX1 3PH, United Kingdom

[§]Biochemistry Department, University of Oxford, South Parks Road, Oxford, OX1 3QU, United Kingdom

[¶]National Institute for Chemical Physics and Biophysics, Akadeemia Tee 23, Tallinn, Estonia

Keywords: Biomolecules · DFT · DOR · High-Resolution · MQMAS · NMR Crystallography · Oxygen-17

φ present address: CEA Saclay.

Authors for correspondence:
Mark E. Smith, University of Warwick, E-mail: M.E.Smith.1@warwick.ac.uk; Tel: +44 (0)2476 5 22380; Fax: +44 (0)2476 1 50897
Alan Wong, CEA Saclay, E-mail: alan.wong@cea.fr; Tel: +33 (0)1 69 08 41 05; Fax: +33 (0)1 69 08 98 06
Ray Dupree, University of Warwick, Email R.Dupree@warwick.ac.uk; Tel: +44 (0)2476 523403

Abstract

Monosodium L-glutamate monohydrate, a multiple oxygen site (eight) compound, is used to demonstrate that a combination of high-resolution solid-state NMR spectroscopic techniques open up new possibilities for ^{17}O as a nuclear probe of biomolecules. Eight oxygen sites have been resolved by double rotation (DOR) and multiple quantum (MQ) NMR experiments, despite the ^{17}O chemical shifts lying within a narrow shift range of <50 ppm. ^{17}O DOR NMR not only provides high sensitivity and spectral resolution, but also allows a complete set of the NMR parameters (chemical shift anisotropy and electric-field gradient) to be determined from the DOR spinning-sideband manifold. These ^{17}O NMR parameters provide an important multi-parameter comparison with the results from the quantum chemical NMR calculations, and enable unambiguous oxygen-site assignment and allow the hydrogen positions to be refined in the crystal lattice. The difference in sensitivity between DOR and MQ NMR experiments of oxygen in bio/organic molecules is also discussed. The data presented here clearly illustrates that a high resolution ^{17}O solid-state NMR methodology is now available for the study of biomolecules, offering new opportunities for resolving structural information and hence new molecular insights.

Introduction

Solid-state nuclear magnetic resonance (NMR) spectroscopy has been used to make significant strides in recent years in molecular structure determinations (refs to reviews); high-resolution NMR spectra can be obtained routinely for spin-½ nuclei such as ^{1}H, ^{13}C and ^{15}N in complex systems, such as biomolecules and organic complexes. Connectivity between such nuclei can readily be probed through either dipolar or scalar couplings in 1D or 2D correlation experiments, and, with the improvements in the first-principle quantum chemical calculations and computing resources – a new discipline in NMR spectroscopy 'NMR crystallography' is rapidly emerging.[1,2,3] The concept is to provide detailed structural information about a solid material using complementary NMR techniques and calculations. To date, the applications of NMR crystallography have mainly concerned spin-½ nuclei, e.g. ^{1}H, ^{13}C, ^{15}N and ^{29}Si.[1-4] This is because high spectral resolution of spin-½ systems can be obtained from routine magic-angle spinning (MAS) experiments, such that different sites can readily be resolved and as a result the chemical shift measurements for different crystallographic sites are straightforward. The high spectral resolution together with shielding (i.e. chemical shift) calculations can provide valuable structural insight.

In contrast the quadrupole interaction often significantly broadens the NMR signal of nuclei with spin > ½.[5] This greatly hinders the spectral resolution, even under fast MAS, for a molecular system with multiple crystallographic sites preventing spectral assignment. Oxygen, like carbon and nitrogen, is one of the core elements in bio/organic molecules and is involved in many structural and physiological functions. However the large quadrupole interaction in ^{17}O (spin-5/2) in bio/organic molecules,[6,7] combined with the low natural abundance (0.037 %), make it challenging to acquire high spectral resolution spectra that allow site-specific information to be unambiguously extracted from a multiple-site system.

Different high-resolution NMR approaches for suppressing the quadrupole broadening have been developed: multiple-quantum (MQ) MAS[8,9] and later satellite-transition (ST) MAS[10,11] both of which rely on manipulation of spin-coherences by radio-frequency (rf) pulses; and double-rotation (DOR)[12,13] and dynamic-angle spinning (DAS)[12] rely on manipulation of the spatial tensors by sophisticated sample spinning. The method of choice is a matter of strategy and availability, since these methods are either technically sophisticated and/or exhibit reduced sensitivity. MQMAS and STMAS provide information on both the isotropic and anisotropic quadrupolar interaction, but the drawbacks are the intrinsic weak sensitivity and time consuming two-dimensional (2D) signal acquisition. DOR and DAS, in turn, require specialised probes. Like MQMAS and STMAS, DAS is an indirect approach to high-resolution solid-state NMR because it is a 2D experiment. Despite the low filling factor as a result of the inner rotor needing to spin within a large rotor diameter and the consequent slow spinning, DOR is a direct approach to high-resolution solid-state NMR for quadrupolar nuclei. It is intrinsically a 1D solid-state NMR experiment. Furthermore it has the advantage that the chemical shift anisotropy can be readily obtained.[17] With the advances in quadrupole NMR methodologies, a significant increase in ^{17}O NMR studies of bio/organic materials have been reported recently,[6,7] including a high-field ^{17}O solid-state NMR study of two large (64 and 80 kDa) protein-ligand complexes,[14] illustrating the potential of ^{17}O NMR spectroscopy toward large biological systems. In particular, recent demonstrations on ^{17}O DOR spectroscopy have reported ultra-high spectral resolution with linewidths of <1 ppm).[15-21]

It is worth noting that high-resolution ^{17}O NMR MQMAS and DOR have also been reported for many important inorganic materials.[5,22-24] In comparison to inorganic materials, there are three major complications for ^{17}O solid-state NMR on bio/organic molecules: (1) the abundance of hydrogen in bio/organic molecules gives rise to significant dipolar broadening unless high power ^{1}H-decoupling is applied; (2) the quadrupole interaction is generally larger (7–10 MHz) in bio/organic molecules[6,7] than

in most inorganic materials (<6 MHz);[5,22] and (3) there are often, more crystallographically inequivalent sites present in bio/organic molecules potentially over a more limited chemical shift range compared to inorganic materials, thereby increasing spectral crowding. These three factors make high-resolution ^{17}O solid-state NMR studies on bio/organic systems a significant challenge such that this technique has yet to be applied to NMR crystallography of bio/organic molecules.

In this study we combine multiple-field ^{17}O DOR and MQMAS NMR experiments with density functional theory (DFT) calculations to provide spectral assignment of all the crystallographic sites in a representative simple biomolecule, monosodium L-glutamate monohydrate (MSG). MSG is known as a flavour enhancer, which has been used for nearly a century to bring out the flavour in foods. Its principal molecular component is an amino acid called L-glutamate, in which carboxylate oxygens are the important functional groups. The crystal lattice consists of two crystallographically distinct MSG molecules.[25] The similar, but inequivalent eight oxygen sites provides a testing challenge for solid-state ^{17}O NMR spectroscopy. A previous short communication simply reported the ability to resolve seven isotropic ^{17}O NMR resonances within a ~50 ppm shift range,[19] with no detailed extraction of the NMR interaction parameters and only a tentative spectral assignment, based upon the effect of ^{1}H decoupling on the observed linewidths and no DFT results.

This study very much extends the initial single field MAS and DOR data, combining multiple field DOR and 3QMAS together with computational NMR data for the first time to provide unequivocal ^{17}O site assignment and structural refinement (H-atoms in particular) of a 'bio/organic' solid. This demonstrates the utility of high-resolution ^{17}O solid-state NMR spectroscopy in a multi-parameter analysis that is not available to spin-½ systems because of the additional NMR interactions present for a quadrupolar nucleus.

Experimental Section

Sample preparation. The starting material [^{17}O]-labelled L-glutamic acid was prepared according to a previously described procedure[26] using 20% ^{17}O-atom enriched $H_2[^{17}O]$. Monosodium L-glutamate·monohydrate (MSG) was prepared by dissolving [^{17}O]-L-glutamic acid in cold water and neutralized with NaOH(aq). The white crystalline powder used for NMR experiments was recrystallised at room temperature.

NMR experiments. ^{17}O solid-state NMR experiments were carried out on Chemagnetics Varian Infinity 600 and 800 spectrometers at frequencies of 81.37 and 108.36 MHz, respectively. Varian 4.0 and 3.2 mm T3 MAS probes were used for ^{17}O MAS and triple-quantum (3Q) MAS NMR experiments. Sample spinning at 12000–15000 Hz with XiX ^{1}H-decoupling (^{1}H rf ~80 kHz) were used for recording MAS and 3QMAS NMR spectra. A rotor-synchronised full spin-echo experiment was performed to record a 1D MAS spectrum with ~100,000 transients and a recycle delay of 0.5 s. A phase-modulated split-t_1 3QMAS[27] experiment was carried out to acquire the 2D spectra at 14.1 and 18.8 T. At 14.1 T, the optimised excitation pulse (P1) was 6.0 μs with fast-amplitude-modulated (FAM)[28] conversion pulses (P2) of 1.2, 0.8, 0.7, 0.6 μs (^{17}O rf ~90 kHz). A total of 4800 transients were collected for each of the 360 t_1 increments, with a t_1 dwell time of 25 μs and a recycle delay of 0.2 s. At 18.8 T, the P1 pulse was 4.2 μs and the FAM P2 pulses were 1.0, 0.7, 0.6 and 0.5 μs (^{17}O rf ~90 kHz). A total of 3456 transients were collected for each of the 478 t_1 increments, with a t_1 dwell time of 20 μs and a recycle delay of 0.2 s. ^{17}O DOR NMR spectra were acquired using a single-pulse odd-order sideband suppression experiment[29,30] with a continuous-wave ^{1}H-decoupling (^{1}H rf 30–55 kHz) on custom-made DOR probes. DOR NMR spectra at various outer-rotor spinning frequencies (ν_{OR} = 1500–1900 Hz) were recorded to identify the isotropic peaks. A recycle delay of 0.5 or 1.0 s was used. All ^{17}O NMR spectra were reference to H_2O at 0 ppm. ^{13}C and ^{1}H NMR experiments were performed on a Bruker

Avance II$^+$ 600 with a Bruker 4-mm MAS probe spinning at 12500 Hz frequency. ^{1}H and ^{13}C spectra were acquired with a standard 1D windowed-DUMBO[31] and a CP/MAS pulse sequence, respectively. ^{1}H and ^{13}C chemical shifts were referenced to TMS (0 ppm) and L-alanine (CH_3: 20.5 ppm), respectively. The ^{17}O DOR spectral simulation was performed by numerical density matrix simulations.[17]

NMR computational method. The calculations were performed within Kohn-Sham Density Functional Theory using the CASTEP code.[32] This is able to treat infinitely periodic solids by using the translational symmetry inherent in crystals and simulating the crystallographic unit cell under periodic boundary conditions. For all calculations the Perdew-Burke-Ernzerhof (PBE) generalised gradient approximation[33] was used. The interaction between the valence electrons, and the nuclei and core electrons was described using ultrasoft pseudopotentials.[34] The wave functions are expanded on a plane-wave basis set with a maximum kinetic energy of 1000 eV, and integrals over the electronic Brillouin zone used a minimum *k*-point spacing of 0.01 Å^{-1}. It is worth noting that increasing both the density of the *k*-point sampling and the maximum plane-wave energy gave practically identical NMR parameters. Calculations using the original X-ray crystal structure[25] gave unrealistically large forces for the X-ray determined hydrogen positions indicating that they were incorrect. For this reason, the ^{17}O NMR calculations were carried out on several structurally optimised MSG models: (1) a H-optimised structure for which only the hydrogen atoms were relaxed; (2) a O,H-optimised for which both oxygen and hydrogen atoms were relaxed; and (3) a fully optimised situation where all atoms are relaxed. In all cases, the structural optimisation originated from the X-ray crystal structure and the unit cell parameters were constrained to the original values found in the X-ray structure.

The shielding (σ) and electric-field gradient (EFG) tensors were computed using the GIPAW[35,36] and PAW,[37] respectively. For chemical shift comparison between the experimental values

and the computed results, the calculated shielding are converted to chemical shift (δ) using $\delta = \sigma_{ref} - \sigma_{sample}$, where σ_{sample} and σ_{ref} are the absolute shielding for the nucleus of interest and for the reference nucleus, respectively. In this study, we use the following σ_{ref}: $\sigma_{ref}(^{17}O$, full- and O,H-optimised) = 237 ppm, $\sigma_{ref}(^{17}O$, H-optimised and X-ray) = 245 ppm, $\sigma_{ref}(^{1}H)$ = 30.7 ppm, and $\sigma_{ref}(^{13}C)$ = 169.8 ppm.

Results and Discussion

^{17}O MAS. As shown in Figure 1A, the X-ray crystallographic study[23] of MSG shows that there are two distinct L-glutamate molecules in the crystal lattice, resulting in a total of eight different carboxylate oxygen sites. All eight oxygen sites have very similar local environments; each has one σ_{C-O} covalent bond and interacts with the neighbouring hydrogen atoms and/or sodium ions. On this basis one would expect the oxygen sites to have similar ^{17}O NMR parameters (i.e. chemical shift and electric-field gradient), such that it would be difficult to resolve the eight distinct oxygens using the conventional solid-state NMR experiment, MAS. Indeed Figure 1B shows a broad ^{17}O MAS signal centred at 220 ppm with a linewidth ~8000 Hz. This signal arises from the eight overlapping second-order quadrupolar broadened signals. Although the observed MAS resonance exhibits many sharp singularities and distinct discontinuities, deconvolution of the ^{17}O MAS spectrum is impractical even considering spectra recorded at multiple magnetic fields.

^{17}O 3QMAS. In contrast, the ^{17}O 3QMAS spectra (Figure 2) show significant improvement in resolution by successfully removing the second-order quadrupole broadening, resulting in narrow isotropic 3Q peaks (Q1-Q7) along the 3Q projection, Figure 2A. Five distinct 3Q isotropic peaks are resolved in the 3QMAS spectrum recorded at 14.1 T, and seven at 18.8 T (Table 1). Note that in Figure 2B the isotropic 3Q peaks are not the dominant signals in both 14.1 and 18.8 T 3Q projected spectra, and that the observed spinning-sideband manifolds extend over a large range (> 600 ppm), particularly

at 18.8 T, indicating the presence of significant chemical shift anisotropy (CSA) at the oxygen sites. In principle, the projected MAS slices obtained from the summation of all sidebands (shown in Figure 2A) give an estimation of χ_q (quadrupolar coupling constant) and η_q (quadrupolar asymmetry parameter – see ref. 38 and below for the definition). However the rather poor MAS lineshapes observed are not good enough to determine these parameters to better than ~0.5 MHz and ~0.1, respectively.

A large number of t_1 steps, which extended to 9+ ms, were required to acquire the high-resolution spectra along the 3Q projection. The observed 3Q linewidths were found to be about 150 Hz, narrower lines could possibly have been achieved by extending the t_1 period. However, this would be a very time consuming experiment, particularly for ^{17}O in biomolecules where a large χ_q is expected. Even though the ^{17}O spin relaxation time for MSG is relatively short, which enables fast signal-averaging, four days of acquisition were needed to acquire the ^{17}O 3QMAS spectra shown in Figure 2, thus a much longer time would be needed to further improve either the spectral-resolution or the signal-to-noise.

^{17}O DOR. Figure 3 shows ^{1}H-decoupled ^{17}O DOR spectra at 14.1 and 18.8 T. Both spectra clearly exhibit a great improvement in resolution compared to MAS. The DOR isotropic shifts (δ_{DOR}) were identified by varying the outer-rotor spinning frequency, and seven isotropic peaks (P1-P7) were found (Table 1). The intensity for P1 is approximately twice that of the other peaks suggesting that P1 corresponds to two oxygens, thus all eight oxygens in MSG are accounted for in the ^{17}O DOR spectrum. A linewidth of ~70 Hz at 14.1 T is achieved by ^{1}H-decoupling. Although both 3QMAS and DOR produce sufficient line-narrowing for high-resolution spectra, DOR gives much better signal sensitivity as it is a 1D experiment. A good DOR spectrum can be acquired in a few hours, a much shorter time than the four days acquisition of the 2D 3QMAS spectra. This significant gain in signal

sensitivity is because the DOR spectrum is acquired in real time, where the second-order quadrupolar broadening effect is averaged by spinning the sample at two different axes simultaneously, allowing for 1D spectral acquisition. Hence comparing DOR to 3QMAS two advantages of the former need to be considered (i) the much shorter timescale required to acquire the data set with sufficient resolution and (ii) the intrinsic the lower signal sensitivity of the 3Q experiment as a result of the typically weaker excitation of the triple-quantum transitions compared to the single quantum ones.

It should be noted that the ^{17}O DOR spectra of MSG acquired in this study use a rather low ^{17}O isotopic enrichment of only 20%. Thus, DOR could be used to probe the oxygen atoms in larger biomolecules with higher ^{17}O isotopic enrichment and with simple pulse-enhancement technique.[21] Currently, we are working on ^{17}O DOR detection of larger protein molecules with selective ^{17}O-labelling sites.

Determination of site-specific ^{17}O solid-state NMR interaction parameters. The main nuclear interactions for ^{17}O are the chemical shift (CS) and the quadrupole interaction with the electric-field gradient (EFG). The CS tensor components (δ_{11}, δ_{22}, δ_{33}) can be written in terms of span Ω and skew κ as:

$$\delta_{iso}\,[\text{ppm}] = {}^{1}/_{3}\,(\delta_{11} + \delta_{22} + \delta_{33}) \qquad (\delta_{11} \geq \delta_{22} \geq \delta_{33}) \qquad [1]$$

$$\Omega\,[\text{ppm}] = \delta_{11} - \delta_{33} \qquad (\Omega \geq 0) \qquad [2]$$

$$\kappa = 3\,(\delta_{22} - \delta_{iso}) / \Omega \qquad (-1 \leq \kappa \leq +1) \qquad [3]$$

The quadrupole interaction is described by a coupling constant $\chi_q = e^2Qq_{zz} / h$, where Q is the nuclear quadrupole moment[39] and an asymmetry parameter $\eta_q = (q_{xx} - q_{yy}) / q_{zz}$ where $0 \leq \eta_q \leq 1$. The relative orientation between the CS and EFG tensors is described by three Euler angles (α, β, γ). Traditionally, the above parameters can be efficiently extracted from multiple field static and MAS spectra, combined with high-resolution MQMAS spectra for more complicated multiple site systems. To date, in no

system with more than four oxygen sites in a bio/organic molecule have all the oxygen sites been resolved and the complete set of ^{17}O NMR parameters successfully determined.[6,7] However, due to the complexity of the spectrum with eight oxygen sites in MSG the determination of all the NMR parameters cannot rely on static, MAS and MQMAS spectra alone, additional complementary methods are required. The δ_{3Q} and δ_{DOR} shifts exhibit an opposite field dependency, and can be conveniently presented on a 3Q/DOR plot,[40] where the vertical axis positions depend upon the 'negative' or 'positive' inverse square of the resonance frequency ν_o. For ^{17}O with I = 5/2,

$$\delta_{DOR}\,[\text{ppm}] = \delta_{iso}\,[\text{ppm}] - \frac{3}{500}\frac{P_q^2}{\nu_o^2}\times 10^6 \qquad [4]$$

$$\delta_{3Q}\,[\text{ppm}] = \delta_{iso}\,[\text{ppm}] + \frac{3}{850}\frac{P_q^2}{\nu_o^2}\times 10^6 \qquad [5]$$

$$\text{where} \quad P_q[\text{MHz}] = \chi_q\sqrt{1+\frac{\eta_q^2}{3}} \qquad [6]$$

the ^{17}O NMR parameters, δ_{iso} and P_q, for each observed δ_{DOR} peak can be determined from the slope (P_q) and the ordinate (δ_{iso}) of the field dependency 3Q/DOR plot (Figure 4A). The MAS projected lineshapes from the 3QMAS spectra (Figure 2A) showed that η_q is ~0.45 for all sites, however because of the clear spectral singularities/discontinuities features in the MAS spectrum at 14.1 T (Figure 1B), the accuracy of δ_{iso}, χ_q and η_q can further be improved by simulating the spectrum using the accumulated information determined from the above 3Q/DOR plot and the observed δ_{DOR} shifts. The resultant fitted MAS spectrum (Figure 4B) gives an excellent agreement with the experiment, indicating the high accuracy of the data obtained. In addition, as shown in Figure 4B, each DOR isotropic peak (P1-P7) is flanked by a set of spinning-sidebands that carry information on a 7-dimensional parameter space: Ω, κ, χ_q, η_q and (α, β, γ). These parameters describe the magnitude and

relative orientation of the CS and EFG tensors. To aid fitting the DOR spectrum we performed extensive DFT NMR calculations based on the MSG structure. The DFT results suggest that the Euler angle β is approximately –90° for all eight oxygen sites; hence β was constrained at –90° for the DOR spectral fitting. With this additional information, the DOR spectral simulation is now reduced to a 4-dimensional parameter space (Ω, κ, α and γ). By carefully fitting the sideband manifolds for each corresponding δ_{DOR} peak with these remaining 4 parameters, we were able to determine a complete set of ^{17}O NMR parameters for all eight oxygens in MSG. The accuracy of the NMR parameters was improved by a simultaneous fit of the DOR spectra at different spinning frequencies and applied fields. The results are summarised in Table 2 and compared with the DFT results for a O,H-optimised structure. These results represent the first set of full NMR parameters extracted for a biomolecule with more than four oxygen sites.

Due to the complexity of determining the ^{17}O NMR parameters, uncertainties of the data are unavoidable. These can be attributed to various sources: (1) the errors in δ_{iso} and P_q from fitting in the 3Q/DOR plot; (2) the constraints on η_q and β which were determined from the 3QMAS spectra and the DFT calculation, respectively; (3) identical sideband manifolds can be produced from multiple combinations of parameters; and (4) for P1, the uncertainty will be greater than for the others since it arises from two unresolved oxygens, which might have different parameters; however the excellent agreement between the simulations and experiment for both MAS and DOR spectra (Figure 4B) indicate that the errors are small. They are estimated to be: ±1 ppm for δ_{iso}, ±20 ppm for Ω, ±0.1 for κ, ±0.2 MHz for χ_q, and ±5° for α and γ.

It should be strongly emphasised that without the knowledge of δ_{iso}, P_q from the field dependent 3Q/DOR study and β from the DFT calculation, it would be difficult to uniquely simulate the DOR spectra and extract the CS and EFG data for each oxygen site in MSG. The complementary nature of

DOR and MQMAS experiments and with DFT calculations performed here demonstrates their utility for determining site-specific NMR parameters of a complex multiple site system.

Spectral assignment and structural refinement. Up until now, we have only described the step-by-step procedures to extract accurate and reliable ^{17}O NMR parameters from a system showing multiple closely related oxygen sites, but the question remains 'what are the correct spectral assignments?' As mentioned earlier, the local environments of the carboxylate oxygens in MSG are very similar to one another. The small structural differences hinder definitive spectral assignment. A tentative assignment was made previously[19] based solely on the individual DOR linewidth, assumed now to be due to residual ^{1}H dipolar coupling, together with the X-ray structural information (where the proton positions are uncertain): O11 and O12 to P1; O1 or O2 to P2; O3 or O13 to either P3 or P4; O1 or O2 to P5; O4 and O14 to either P6 or P7. In recent years ^{17}O NMR calculations have become a valuable complementary tool for spectral analysis.[6,7] Hence, to assist in the spectral assignments, extensive DFT calculations on MSG have been carried out. Hydrogen positions from X-ray data are often inaccurate leading to large discrepancies in the parameters calculated using DFT methods. This is especially true for oxygen sites involved in strong hydrogen-bonds. To minimise any uncertainties from the DFT results, the NMR calculations were performed on the X-ray structure and on different MSG models: H-optimised, O,H-optimised and fully-optimised structures. Since the object is to assign the peaks, the absolute shielding reference σ_{ref} was determined by minimising the standard deviation of the calculation from measured chemical shifts. The value is slightly different for these MSG models being 245 ppm for X-ray and H-optimised structures, and 237 ppm for O,H- and fully-optimised structures. A summary of the DFT ^{17}O NMR results for these MSG models are reported in Table 3, and a complete list of the local O···H bond distances of each oxygen site is summarized in Table 4. The resultant DFT NMR results can be used in combination with the experimental values extracted from DOR sidebands,

including ^{17}O CSA span (Ω), for an ambiguous spectral assignment. Figure 5B shows a 3-dimensional (δ_{iso}, P_q and Ω) comparison of the experimental values with the DFT results from the X-ray data and the O,H-optimised model. This 3D comparison clearly allows for site assignments since the experimental data and the DFT results are clustered. Figures 5C and 5D display a 2D comparison with all DFT structural models. Based on these comparisons, it suggeste that the observed higher intensity for P1 in the DOR spectra corresponds to two oxygen atoms, O2 and O12, which have similar ^{17}O NMR parameters (see Table 2). One possible approach to spectrally resolve O2 and O12 would be MQ-DOR,[41] a combined technique of DOR and MQMAS, at high magnetic field. It should be pointed out that the DFT Ω and P_q values used in both the 2D and 3D comparisons are scaled by 0.76 and 0.93, respectively, since the DFT results are systematicallyoverestimated by about 24% and 7%, respectively. Overestimation of ^{17}O DFT Ω and P_q have been reported for other biomolecules,[42,43] indicating that, as with DFT bond length calculations, there are systematic errors in the calculations of these parameters and a very similar scaling factor (0.77) was found for the ^{13}C span in sucrose.[44] One source of the discrepancy in Ω is that the DFT calculations are carried out at 0 K whereas the NMR measurements are at ~300 K. It was shown in Dumez and Pickard[45] that molecular motional effects have a significant influence on shielding anisotropies in organic solids. The differences between the experimental and the DFT results of δ_{iso}, Ω and P_q for different structural MSG model are summarised in Table 5. Note that the DFT results using the X-ray data are in much worse agreement with the experimental values than the optimised models, especially for oxygens O14 and O1. The O,H- and fully-optimised models are in slightly better agreement with the experiment than H-optimised model, with the O,H-optimised model having the smallest standard deviation in $|\Delta\delta_{iso}|$, but with similar deviations in $|\Delta\Omega|$ and $|\Delta P_q|$ to the fully-optimised model.

With the good agreement of ^{17}O NMR parameters between the reliable experimental data and the DFT values of the optimised models, a crystallographically refined structure for MSG is determined (see Figure 5A). The DFT calculations demonstrate a remarkable sensitivity of ^{17}O NMR interaction parameters to the neighbouring hydrogens, as only very subtle differences in H-positions are found between the original X-ray data and the DFT refined models, e.g. for O1 the largest change in distance is 0.05 Å. Even for O14, where the distance of one nearby H changes from 2.061 to 1.796 Å, six other distances change by less than 0.03 Å. A full set of the changes in O…H distances are summarised in Table 4.

Hydrogen-bonding effects. Further confirmation of the spectral assignment comes from analysing the effect of proton dipolar coupling on the DOR linewidths. Figure 6A shows the effects on the DOR linewidth acquired at 18.8 T with and without ^{1}H-decoupling. The linewidths in the ^{1}H-decoupled spectrum (~120–200 Hz at 18.8 T) are nearly a factor of 3 narrower than those in the undecoupled spectrum giving rise to a much higher spectral resolution. For example, P1, P3, P5 and P7 peaks in the decoupled spectrum are well resolved from the neighbouring spinning-sidebands clearly illustrating the importance of ^{1}H-decoupling. Despite the improvement of linewidth, the combination of low ^{1}H-decoupling field (<50 kHz) and slow spinning frequency (1000–2000 Hz) is insufficient to completely remove the stronger O···H dipole contributions resulting in 'residual' dipole broadening for some sites. We have previously shown the effects of different ^{1}H-decoupling power on the residual DOR linewidth of the oxygens in alanine.[20] In another case, we also found that the strong O-H dipole at the hydroxyl oxygen site in glycine·HCl made it virtually invisible in the ^{1}H-decoupled DOR spectrum.[18] For the case of MSG, each oxygen interacts with different numbers of hydrogens and has different hydrogen-bond networks (Table 4); hence, each oxygen experiences a different magnitude of the total O···H dipole contribution, which can be expressed as,

$$< D_{ij} > [\text{Hz}] = \sqrt{\sum D_{ij}^2} \qquad [7]$$

$$\text{where} \quad D_{ij}\ [\text{Hz}] = \left(\frac{\mu_0}{4\pi}\right)\frac{\gamma_O \gamma_H \hbar}{2\pi} < r_{ij}^{-3} >, \qquad [8]$$

r_{ij} is the internuclear separation, and γ is the gyromagnetic ratio of the nuclei. The resulting $<D_{OH}>$ are shown in parentheses in Table 4. Figure 6B displays the correlation between $<D_{OH}>$ and the residual linewidth at 14.1 (blue line) and 18.8 T (red line). To be able to compare the linewidth in two different applied fields, the linewidth observed for 14.1 T is normalised to 18.8 T by scaling with the applied field ratio 4/3. The figure clearly shows that the residual linewidth increases as a function of calculated $<D_{OH}>$ and provides additional confirmation of the assignments given earlier. For example both O4 and O14 (which correspond to P7 and P6) have seven O···H distances with <3Å and a strong dipole contribution (~4500 Hz) and, as a result, relatively broad linewidths (~180 Hz) were observed. In contrast $<D_{OH}>$ for O1 and O2 (which correspond to P2 and P1) is significantly smaller (~1900 Hz) and their linewidths (~120-140 Hz) are considerably narrower.

^{17}O, ^{13}C and ^{1}H NMR spectral comparison with DFT. Figure 7 shows that the simulated DOR spectrum using the DFT results from the O,H-optimised model gives a better agreement with the experimental DOR spectrum compared to that from the X-ray model. As discussed earlier, the P_q values used for the DFT simulated spectrum are scaled by 0.93. The DFT spectrum suggests that the overall hydrogen positions in the O,H-optimised model of MSG are better than those in the previous determined X-ray structure.[25] Similar conclusions can also be drawn from the ^{1}H and ^{13}C spectral comparisons. This also points out that the *spectral information available* from the ^{17}O NMR analysis demonstrated in this study is on apar (or better because of the ability of a multi-parameter comparison) with the current-state of ^{1}H and ^{13}C solid-state NMR spectroscopy. Of course, the challenges for

obtaining good ^{17}O NMR signal sensitivity with good spectral resolution are still far greater than those for ^{1}H and ^{13}C NMR.

^{17}O CS and EFG tensors. With the aid of the DFT calculations we have successfully determined the site-specific ^{17}O NMR parameters which provided crucial information for site assignment. Another advantage of the DFT calculation is that it enables an understanding of the chemical environments around the site of interest to be gained. In particular it gives the CS (δ_{11}, δ_{22}, δ_{33}) and EFG ($\chi_{q,xx}$, $\chi_{q,yy}$, $\chi_{q,zz}$) tensor components of the oxygen site in the molecular frame of reference. A summary of the DFT ^{17}O CS and EFG tensors for the carboxylate oxygens in MSG is listed in the supplementary materials, along with a diagram showing the general orientations of the tensor components for carboxylate (O-C-O) and carbonyl (C=O) oxygens. For ^{17}O CS, the smallest CS component, δ_{33}, is found to be perpendicular to the carboxylate plane, whereas the other two CS components, δ_{11} and δ_{22}, lie in the same carboxylate plane. In particular, δ_{22} is about 35° from the C-O bond axis. Similar CS tensor orientations are also found for the carboxylate oxygens in oxalate.[45] However in most cases, the CS tensor orientations in carbonyl oxygen are found to be different from those in carboxylate oxygen. For example, the δ_{11} (and not δ_{22} as in carboxylate) of the carbonyl oxygen, in amino acids,[42] nucleic bases[47] and in peptides[43,48] is approximately 20–30° away from the C=O axis. This difference may be attributed to the different bond characters between C-O and C=O. In contrast to the CS tensor, the EFG tensor orientations for carboxylate oxygens (with the exception of aldehydes and ketones) are similar to those for carbonyl oxygen. $\chi_{q,xx}$ is found to be perpendicular to both the carboxylate and carbonyl planes, $\chi_{q,yy}$ and $\chi_{q,zz}$ lie in the plane with $\chi_{q,yy}$ nearly parallel to the C-O and C=O bond axes, respectively. The relative orientation between the CS and EFG tensors, described by the Euler angles (α, β, γ), has one common feature for both carboxylate and carbonyl oxygens. It is found that β is always very close to –90° or +90°. This is greatly beneficial for the spectral analysis, because with β =

±90° the simulations corresponding to +γ and –γ (and to 180 – γ) are nearly identical, as are those with α (see supplementary material). Consequently the angular range to be varied for both α and γ reduces to 0° to ±90° and the fitting for carboxylate and carbonyl oxygens is simplified.

Conclusion

We have determined the site-specific ^{17}O CS and EFG tensors for all eight oxygen sites in a biomolecule by an extensive complementary approach using multiple-field DOR and 3QMAS experiments together with DFT calculations. We found that unambiguous spectral assignment can be made for such a complex system by simply comparing the measured ^{17}O δ_{iso}, Ω and P_q parameters with the DFT results (i.e. a 3-dimentional NMR parameters comparison). The spectral assignment was confirmed by the O-H dipolar coupling behaviour. The results here represent the first high spectral resolution ^{17}O solid-state NMR study on a complex biomolecule where full site assignment is made, and a complete set of ^{17}O NMR parameters is determined for each site. The results also represent a significant development towards ultra high-resolution for ^{17}O solid-state NMR spectroscopy, where resolution is now comparable to that for spin-½ nuclei. We have also demonstrated that the sensitivity in the DOR spectra is considerably better than those in 3QMAS spectra. In principle, the sensitivity in DOR could be further enhanced by implementing an inductively couple detector[49] inside the sample volume to dramatically increase the filling factor (from ~0.3 to almost 1). Moreover, the availability of high rf strength[50] from the inductive detector could benefit the MQ-DOR experiment[41] for ^{17}O nuclei in sites with a large quadrupole interaction, such as in most bio/organic molecules.[6,7] With the current advances in DOR technique and in NMR applications, we anticipate more complex oxygen systems will be characterised by ^{17}O double-rotation NMR spectroscopy, especially coupled with DFT

calculations allowing the ^{17}O NMR crystallography approach to be genuinely extended in such organic molecules from spin-½ nuclei (e.g. ^{1}H, ^{13}C and ^{15}N).[1]

Acknowledgment. We gratefully acknowledge the contribution of Dr V. Lemaître for synthesizing the ^{17}O-enriched L-MSG. This work was supported by EPSRC, BBSRC (BB/C000471/1), the University of Warwick and the Estonian Science Foundation. AW would like thank NSERC of Canada for a Post-Doctoral Fellowship. RD thanks the Leverhulme Trust for funding and an Emeritus Fellowship and JRY thanks Corpus Christi College, Cambridge for a research fellowship.

References

1. R. K. Harris, R. E. Wasylishen and M. J. Duer, *NMR Crystallography*, Wiley, Oxford, 2009.

2. R. K. Harris, *Solid State Sci.*, 2004, **6**, 1025-1037.

3. K. Varga, L. Aslimovska, I. Parrot, M. –T. Dauvergne, M. Haertlein, T. Forsyth and A. Watts, Biochim. *Biophys. Acta*, 2007, **1768**, 3029-3035.

4. D. H. Brouwer, *J. Am. Chem. Soc*., 2008, **130**, 6306-6307.

5. K. J. D. MacKenzie and M. E. Smith, *Multinuclear Solid State NMR of Inorganic Materials*, Pergamon Press, Oxford, 2002.

6. G. Wu, *Prog. Nucl. Magn. Reson. Spectrosc.*, 2008, **52**, 118-169.

7. V. Lemaître, M. E. Smith and A. Watts, *Solid State Nucl. Magn. Reson.*, 2004, **26**, 215-235.

8. L. Frydman and J. S. Harwood, *J. Am. Chem. Soc*., 1995, **117**, 5367-5368.

9. A. Medek, J. S. Harwood and L. Frydman, *J. Am. Chem. Soc*., 1995, **117**, 12779-12787.

10. Z. H. Gan, *J. Am. Chem. Soc.*, 2000, **122**, 3242-3243.

11. S. E. Ashbrook and S. Wimperis, *Prog. Nucl. Magn. Reson. Spectrosc.*, 2004, **45**, 53-108.

12. A. Llor and J. Virlet, *Chem. Phys. Lett.*, 1988, **152**, 248-253.

13. A. Samoson, E. Lippmaa and A. Pines, *Mol. Phys.*, 1988, **65**, 1013-1018.

14. J. Zhu, E. Ye, V. Terskikh and G. Wu, *Angew Chem. Int. Ed.*, 2010, **49**, 8399-8402.

15. A. Wong, K. J. Pike, R. Jenkins, G. J. Clarkson, T. Anupõld, A. P. Howes, D. H. G. Crout, A. Samoson, R. Dupree and M. E. Smith, *J. Phys. Chem. A*, 2006, **110**, 1824-1835.

16. A. Wong, M. E. Smith, V. Terskikh and G. Wu, *Can. J. Chem.*, 2011. Accepted Manuscript.

17. I. Hung, A. Wong, A. P. Howes, T. Anupõld, J. Past, A. Samoson, X. Mo, G. Wu, M. E. Smith, S. P. Brown and R. Dupree, *J. Magn. Reson.*, 2007, **188**, 246-259.

18. A. Wong, I. Hung, A. P. Howes, T. Anupõld, J. Past, A. Samoson, S. P. Brown, M. E. Smith and R. Dupree, *Magn. Reson. Chem.*, 2007, **45**, S68-S72.

19. A. Wong, A. P. Howes, K. J. Pike, V. Lemaître, A. Watts, T. Anupõld, J. Past, A. Samoson, R. Dupree and M. E. Smith, *J. Am. Chem. Soc.* 2006, **128**, 7744-7745.

20. K. J. Pike, V. Lemaître, A. Kukol, T. Anupõld, A. Samoson, A. P. Howes, A. Watts, M. E. Smith and R. Dupree, *J. Phys. Chem. B*, 2004, **108**, 9256-9263.

21. A. Howes, T. Anupõld, V. Lemaitre, A. Kukol, A. Samoson, A. Watts, M. E. Smith and R. Dupree, *Chem. Phys. Letts.*, 2006, **421**, 42-46.

22. S. E. Ashbrook and M. E. Smith, *Chem. Soc. Rev.*, 2006, **35**, 718-735.

23. A. Wong, A. P. Howes, B. Parkinson, T. Anupõld, A. Samoson, D. Holland and R. Dupree, *Phys. Chem. Chem. Phys.*, 2009, **11**, 7061-1068.

24. L. M. Bull, B. Bussemer, T. Anupõld, A. Reinhold, A. Samoson, J. Sauer, A. K. Cheetham and R. Dupree, *J. Am. Chem. Soc*., 2000, **122**, 4948-4958.

25. C. Sano, N. Nagshima, T. Kawakiat and Y. Itaka, *Anal. Sci.*, 1989, **5**, 121-122.

26. V. Lemaître, K. J. Pike, A. Watts, T. Anupõld, A. Samoson, M. E. Smith and R. Dupree, *Chem. Phys. Lett.*, 2003, **371**, 91-97.

27. S. P. Brown and S. Wimperis, *J. Magn. Reson.*, 1997, **128**, 42-61.

28. P. K. Madhu, A. Goldbourt, L. Frydman and S. Vega, *Chem. Phys. Lett.*, 1999, **307**, 41-47.

29. A. Samoson and E. Lippmaa, *J. Magn. Reson.*, 1989, **84**, 410-416.

30. A. Samoson and J. Tegenfeldt, *J. Magn. Reson. A*, 1994, **110**, 238-244.

31. A. Lesage, D. Sakellariou, S. Hediger, B. Elena, P. Charmont, S. Steuernagel and L. Emsley, *J. Magn. Reson.*, 2003, **163**, 105-113.

32. S. J. Clark, M. D. Segall, C. J. Pickard, P. J. Hasnip, K. Refson, M. J. Probert and M. C. Payne, *Zeitschrift fur Kristallographie*, 2005, **220**, 567-570.

33. J. P. Perdew, K. Burke and M. Ernzerhof, *Phys. Rev. Lett.*, 1996, **77**, 3865-3868.

34. D. Vanderbilt, *Phys. Rev. B*, 1990, **41**, 7892-7896.

35. C. J. Pickard and F. Mauri, *Phys. Rev. B*, 2001, **63**, 245101.

36. J. R. Yates, C. J. Pickard and F. Mauri, *Phys. Rev. B*, 2007, **76**, 024401.

37. M. Profeta, F. Mauri and C. J. Pickard, *J. Am. Chem. Soc.*, 2003, **125**, 541-548.

38. M. E. Smith and E. R. H. van Eck, *Prog. Nucl. Magn. Reson. Spectrosc.*, 1999, **34**, 159-201.

39. P. Pyykkö, *Mol. Phys.*, 2001, **99**, 1617-1629.

40. T. Anupõld, A. Reinhold, P. Sarv and A. Samoson, *Solid State Nucl. Magn. Reson.*, 1998, **13**, 87-91.

41. I. Hung, A. Wong, A. P. Howes, T. Anupõld, A. Samoson, M. E. Smith, D. Holland, S. P. Brown and R. Dupree, *J. Magn. Reson.*, 2009, **197**, 229-236.

42. C. Gervais, R. Dupree, K. J. Pike, C. Bonhomme, M. Profeta, C. J. Pickard and F. Mauri, *J. Phys. Chem. A*, 2005, **109**, 6960-6969.

43. E. Y, Chekmenev, K. W. Waddell, J. Hu, Z. Gan, R. J. Wittebort and T. A. Cross, *J. Am. Chem. Soc.*, 2006, **128**, 9849-9855.

44. L. Shao, J. R. Yates and J. J. Titman, *J. Phys. Chem. A*, 2007, **111**, 13126-13132.

45. J. –N. Dumez and C. J. Pickard, *J. Chem. Phys.*, 2009, **130**, 104701-104708.

46. A. Wong, G. Thurgood, R. Dupree and M. E. Smith, *Chem. Phys.*, 2007, 144-150.

47. I. C. M. Kwan, X. Mo and G. Wu, *J. Am. Chem. Soc.*, 2007, **129**, 2398-2407.

48. K. W. Waddell, E. Y. Chekmenev and R. J. Wittebort, *J. Phys. Chem. B*, 2006, **110**, 22935-22941.

49. J.F. Jacquinot and D. Sakellariou, *Conc. Magn. Reson. A* 2011, **38**, 33-51.

50. M. Inukai and K. Takeda, *Conc. Magn. Reson. B* 2008, **33**, 115-123.

Figure Captions:

Figure 1. (A) Asymmetric unit of L-MSG. Oxygen and sodium atoms are represented by red and blue sphere, respectively. The oxygen labels correspond to the X-ray structure.[25] (B) ^{17}O MAS NMR spectrum at 14.1 T with sample spinning at 15 kHz. ssb represents the spinning-sidebands.

Figure 2. (A) A 2D ^{1}H-decoupled 3QMAS NMR spectrum at 18.8 T. The spectral region is indicated by the dotted box in B. The summation of the selected MAS projections are shown by the side of the 2D spectrum. (B) The 3Q projection spectra at 14.1 and 18.8 T. Q1-Q7 are the positions of δ_{3Q}.

Figure 3. ^{1}H-decoupled ^{17}O DOR NMR spectra at 18.8 and 14.1 T. P1-P7 are the positions of δ_{DOR}. The detailed experimental parameters are given in the experimental section.

Figure 4. (A) A magnetic field dependent 3Q/DOR plot. It displays a series of isotropic peaks from DOR and MQMAS measurements at different fields. The ^{17}O DOR spectrum at 8.45 T was acquired at a Bruker Avance using a custom-built probe without ^{1}H-decoupling. (B) Experimental (bottom) and simulated (top) DOR and MAS NMR spectra at various applied fields and rotor spinning frequencies. The δ_{DOR} peaks are indicated by P1-P7.

Figure 5. (A) An overlay of the X-ray and DFT (O,H-optimised model) refined structure of an asymmetric unit of L-MSG. The subtle differences in the H-positions can be seen in the water molecules and in the NH_3 groups. Sodium atoms are not displayed in the asymmetric unit for clarity (B) A 3D representation of the three principal nuclear parameters (δ_{iso}, P_q, Ω) for ^{17}O, showing how the use of all three parameters allows discrimination between sites with similar shifts and comparing the experimental and DFT (X-ray and O,H-optimised model) results. (C) A 2D NMR parameters comparison between Ω *vs* P_q and (D) Ω *vs* δ_{iso}. For the plots B–D, the experimental NMR data are represented by solid red circles; fully optimised model by solid purple; O,H-optimised by solid blue; H-optimised by transparent green; and X-ray structure by transparent brown. In all plots, the DFT Ω and P_q values are scaled by 0.76 and 0.93, respectively. Please see text for details. Other 2D comparisons of NMR parameters can be found in the supplementary materials.

Figure 6. (A) A comparison between the non ^{1}H-decoupled (black) and ^{1}H-decoupled (blue) DOR NMR spectra at 18.8 T with 1615 Hz outer-rotor spinning frequency. ^{1}H rf power at 55 kHz was applied to record the ^{1}H-decoupled spectrum. The upper two spectra display the zoomed region of the bottom two. The isotropic peaks are marked P1-P7, all other peaks are spinning sidebands. (B) The correlation between the ^{1}H-decoupled DOR linewidth and the total O···H dipole contribution (refer to Table 4). The residual linewidth at 14.1 T is normalised to that at 18.8 T by multiplying by the field ratio of 4/3. The O,H-optimised model was used to estimate the average dipole contribution.

Figure 7. High-resolution ^{17}O, ^{1}H and ^{13}C solid-state NMR comparison between the experimental and the DFT results. The ^{17}O DOR NMR spectrum was acquired at 18.8 T, and 1D-windowed DUMBO ^{1}H and ^{13}C CP/MAS spectra at 14.1 T. The DFT ^{1}H and ^{13}C chemical shifts can be found in the supplementary materials. The DFT ^{17}O P_q values (both O,H-optimised and X-ray models) used for the ^{17}O DOR simulations are scaled by 0.93. The δ_{DOR} peaks are indicated by the oxygen-labelled, otherwise are spinning-sidebands.

Table 1. A summary of the observed isotropic peaks in 3QMAS and DOR NMR spectra, and the resulting δ_{iso} and P_q values from a 3Q/DOR plot.

	^{17}O 3QMAS 14.1 T	^{17}O 3QMAS 18.8 T		^{17}O DOR 14.1 T		^{17}O DOR 18.8 T		Results from a 3Q/DOR Plot	
3Q Peak	δ_{3Q} ± 0.5 ppm	δ_{3Q} ± 0.5 ppm	DOR Peak	δ_{DOR} ± 0.5 ppm	$\Delta\nu_{1/2}$ ± 5 Hz	δ_{DOR} ± 0.5 ppm	$\Delta\nu_{1/2}$ ± 5 Hz	δ_{iso} ± 2 ppm	P_q ± 0.1 MHz
Q1	284.1	266.9	P1	195.6	106	219.3	140	251	7.8
Q2	288.5	268.8	P2	204.5	95	227.2	120	256	7.6
Q3	306.4	272.4	P3	213.1	135	237.9	170	269	8.0
Q4	315.8	274.7	P4	220.7	112	245.1	145	274	7.8
Q5	323.5	290.6	P5	222.6	120	247.4	150	276	7.8
Q6	–	300.8	P6	237.8	160	257.7	200	286	7.3
Q7	–	309.5	P7	245.6	150	265.6	180	294	7.4

Table 2. Summary of ^{17}O NMR interaction parameters. Round parentheses represent the DFT results of a O,H-optimised model.

Peak O site	δ_{iso} ±1.0ppm	Ω^a ±20ppm	κ ±0.1	χ_q ±0.2MHz	η_q ±0.10	$P_q{}^a$ ±0.1MHz	α ±5°	β fixed°	γ ±5°
P2	256.0	378	0.45	7.3	0.40	7.49	1	–90	65
O1	*(255.3)*	*(369)*	*(0.44)*	*(7.9)*	*(0.45)*	*(7.65)*	*(1)*	*(–90)*	*(35)*
P4	277.5	400	0.35	7.6	0.45	7.90	5	–90	72
O11	*(279.8)*	*(391)*	*(0.33)*	*(8.4)*	*(0.39)*	*(8.02)*	(6)	*(–90)*	*(40)*
P1	250.7	350	0.40	7.5	0.48	7.78	0	–90	–65
O2	*(249.9)*	*(354)*	*(0.43)*	*(8.0)*	*(0.51)*	*(7.78)*	*(–3)*	*(–88)*	*(–31)*
P1	250.7	350	0.40	7.5	0.48	7.78	0	–90	–65
O12	*(252.9)*	*(354)*	*(0.40)*	*(8.3)*	*(0.50)*	*(8.02)*	*(2)*	*(–89)*	*(–33)*
P3	269.5	300	0.25	7.6	0.50	7.91	0	–90	–65
O3	*(270.4)*	*(311)*	*(0.26)*	*(8.3)*	*(0.51)*	*(8.06)*	*(–2)*	*(–89)*	*(–37)*
P5	280.0	320	0.20	7.7	0.50	8.01	–2	–90	–55
O13	*(279.6)*	*(326)*	*(0.26)*	*(8.4)*	*(0.46)*	*(8.05)*	*(–2)*	*(–89)*	*(–39)*
P7	292.0	340	0.45	6.9	0.45	7.18	5	–90	–65
O4	*(290.4)*	*(343)*	*(0.45)*	*(7.2)*	*(0.56)*	*(7.02)*	*(6)*	*(–90)*	*(–35)*
P6	284.0	330	0.40	6.9	0.45	7.13	–5	–90	60
O14	*(282.8)*	*(331)*	*(0.41)*	*(7.1)*	*(0.62)*	*(7.03)*	*(–6)*	*(–91)*	*(35)*

(a) The DFT values of Ω and P_q have been uniformly scaled by 0.76 and 0.93, respectively.

Table 3. DFT ^{17}O NMR parameters from various MSG models.

Peak	O site	δ_{iso} [a] ppm	Ω [b] ppm	κ	χ_q [b] MHz	η_q	α °	β °	γ °
fully-optimised model									
P2	O1	254.3	490.7	0.44	7.9	0.45	1.0	–90.0	35.3
P4	O11	283.2	518.8	0.33	8.4	0.38	5.6	–89.7	40.3
P1	O2	246.6	461.5	0.44	8.0	0.52	–3.0	–88.3	–31.0
P1	O12	253.0	461.8	0.39	8.3	0.50	1.8	–89.8	–33.0
P3	O3	268.6	408.3	0.25	8.3	0.51	–1.9	–89.0	–37.0
P5	O13	278.1	426.8	0.25	8.3	0.47	–2.3	–89.1	–38.7
P7	O4	289.1	450.1	0.44	7.1	0.56	5.5	–90.0	–35.2
P6	O14	282.6	443.7	0.40	7.1	0.61	–5.4	–90.7	34.8
O,H-optimised model									
P2	O1	255.3	486.2	0.44	7.9	0.45	1.5	–90.0	35.2
P4	O11	279.8	514.7	0.33	8.4	0.39	5.2	–90.3	40.3
P1	O2	249.9	465.4	0.43	8.0	0.51	–2.8	–89.3	–30.5
P1	O12	252.9	465.5	0.40	8.3	0.50	1.6	–90.5	–32.3
P3	O3	270.4	409.9	0.26	8.3	0.51	–1.4	–89.6	–36.2
P5	O13	279.6	428.6	0.26	8.4	0.46	–2.0	–89.7	–39.6
P7	O4	290.4	452.0	0.45	7.2	0.52	5.3	–90.2	–35.1
P6	O14	282.8	435.8	0.41	7.1	0.62	–5.8	–90.2	34.2
H-optimised model									
P2	O1	250.0	474.4	0.43	7.7	0.42	2.5	–89.9	35.6
P4	O11	279.8	508.0	0.34	8.3	0.32	5.0	–89.6	41.5
P1	O2	245.4	456.4	0.43	7.9	0.46	–4.1	–88.0	–32.4
P1	O12	253.0	456.6	0.36	8.2	0.49	2.6	–89.6	–33.4
P3	O3	269.4	401.7	0.26	8.2	0.47	–3.1	–89.4	–37.0
P5	O13	282.8	424.6	0.29	8.3	0.42	–6.1	–89.1	–40.0
P7	O4	290.2	444.1	0.44	7.1	0.55	7.0	–90.4	–32.4
P6	O14	286.4	428.9	0.40	7.1	0.64	–8.6	–89.0	31.9
X-ray model									
P2	O1	248.8	473.0	0.43	7.7	0.42	2.8	–90.1	35.3
P4	O11	277.6	504.6	0.34	8.3	0.33	4.8	–89.3	41.0
P1	O2	245.1	456.0	0.43	7.9	0.45	–3.8	–89.1	–31.2
P1	O12	252.6	455.8	0.35	8.2	0.49	2.8	–89.2	–32.8
P3	O3	269.8	406.1	0.24	8.2	0.48	–2.7	–89.9	–36.3
P5	O13	273.9	416.7	0.25	8.3	0.45	–4.1	–89.3	–38.9
P7	O4	286.3	438.7	0.44	7.1	0.53	6.8	–89.3	–33.6
P6	O14	295.5	459.8	0.43	7.7	0.56	–8.0	–89.5	33.1

(a) $\delta_{iso} = \sigma_{ref} - \sigma_{iso}$, where σ_{ref} = 237 ppm for fully and O,H-optimised models and 245 ppm H-optimised and X-ray models.

(b) The Ω and P_q values are the direct result from the DFT calculation without scaling.

Table 4. A summary of the local O···H distances (<3.0 Å) from X-ray and O,H-optimised structural model. The $<D_{OH}>$ values[a] are given in parentheses.

O1		O2		O3		O4	
X-ray	O,H-opt	X-ray	O,H-opt	X-ray	O,H-opt	X-ray	O,H-opt
2.226	2.245	2.304	2.266	1.791	1.815	1.746	1.770
2.729	2.703	2.553	2.500	2.048	1.831	1.918	1.813
2.854	2.808	2.721	2.723	2.458	2.469	2.560	2.615
3.005	3.000	2.977	2.966	2.900	2.843	2.724	2.723
(2345)	(1913)	(1941)	(2021)	2.918	2.921	2.799	2.785
–	–	–	–	(3704)	(4070)	2.884	2.888
–	–	–	–	–	–	2.849	2.908
–	–	–	–	–	–	(4247)	(4406)
O11		O12		O13		O14	
X-ray	O,H-opt	X-ray	O,H-opt	X-ray	O,H-opt	X-ray	O,H-opt
1.968	1.969	1.874	1.881	1.873	1.803	1.707	1.709
2.276	2.268	2.352	2.332	1.935	1.930	2.061	1.796
2.373	2.386	2.628	2.598	2.476	2.493	2.574	2.546
2.779	2.778	2.708	2.753	2.768	2.779	2.591	2.606
(2922)	(2918)	(3028)	(3019)	2.855	2.842	2.727	2.746
–	–	–	–	(3665)	(3878)	2.883	2.912
–	–	–	–	–	–	2.949	2.975
–	–	–	–	–	–	3.051	2.982
–	–	–	–	–	–	(4221)	(4711)

(a) $< D_{OH} > [\mathrm{Hz}] = \sqrt{\sum D_{OH}^2}$, where D_{OH} is the contribution of O-H dipolar constant.

Table 5. The difference[a] between experimental ^{17}O NMR parameters and DFT calculations.

O site	Fully-optimised model			O,H-optimised model			H-optimised model			X-ray model		
	$\lvert\Delta\delta_{iso}\rvert$ /ppm	$\lvert\Delta\Omega\rvert$[b] /ppm	$\lvert\Delta P_q\rvert$[b] /MHz	$\lvert\Delta\delta_{iso}\rvert$ /ppm	$\lvert\Delta\Omega\rvert$ /ppm	$\lvert\Delta P_q\rvert$ /MHz	$\lvert\Delta\delta_{iso}\rvert$ /ppm	$\lvert\Delta\Omega\rvert$ /ppm	$\lvert\Delta P_q\rvert$ /MHz	$\lvert\Delta\delta_{iso}\rvert$ /ppm	$\lvert\Delta\Omega\rvert$ /ppm	$\lvert\Delta P_q\rvert$ /MHz
O1	1.73	5.01	0.08	0.68	8.52	0.07	5.96	17.46	0.10	7.18	18.50	0.14
O11	5.69	5.72	0.12	2.30	8.83	0.11	2.33	13.90	0.08	0.14	16.53	0.05
O2	4.10	0.73	0.02	0.83	3.67	0.00	5.28	3.14	0.22	5.60	3.44	0.19
O12	2.33	1.00	0.23	2.20	3.76	0.24	2.30	2.97	0.14	1.87	3.60	0.17
O3	0.94	10.27	0.12	0.94	11.53	0.15	0.14	5.31	0.03	0.35	8.63	0.03
O13	1.91	4.39	0.02	0.42	5.74	0.04	2.82	2.68	0.08	6.14	3.28	0.06
O4	2.89	2.12	0.21	1.63	3.51	0.16	1.82	2.49	0.23	5.65	6.60	0.23
O14	1.42	7.26	0.12	1.18	1.22	0.10	2.37	4.00	0.12	11.47	19.42	0.35
SD[c]	1.57	3.27	0.07	0.70	3.47	0.08	1.88	5.82	0.07	3.85	7.03	0.11

(a) |experimental value – DFT value|

(b) the scaled DFT values were used in the comparison: Ω by 0.76 and P_q by 0.93.

(c) SD = $\sqrt{\frac{n\sum x^2 - (\sum x)^2}{n(n-1)}}$

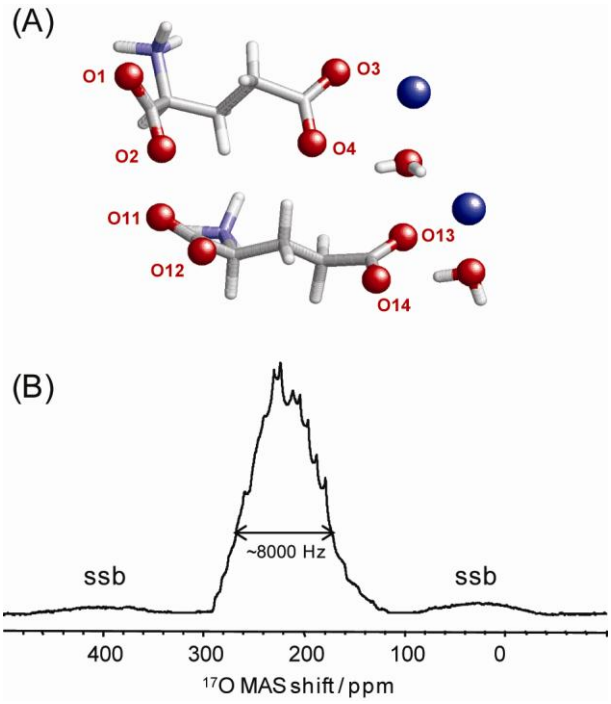

Figure 1. A Wong et al.

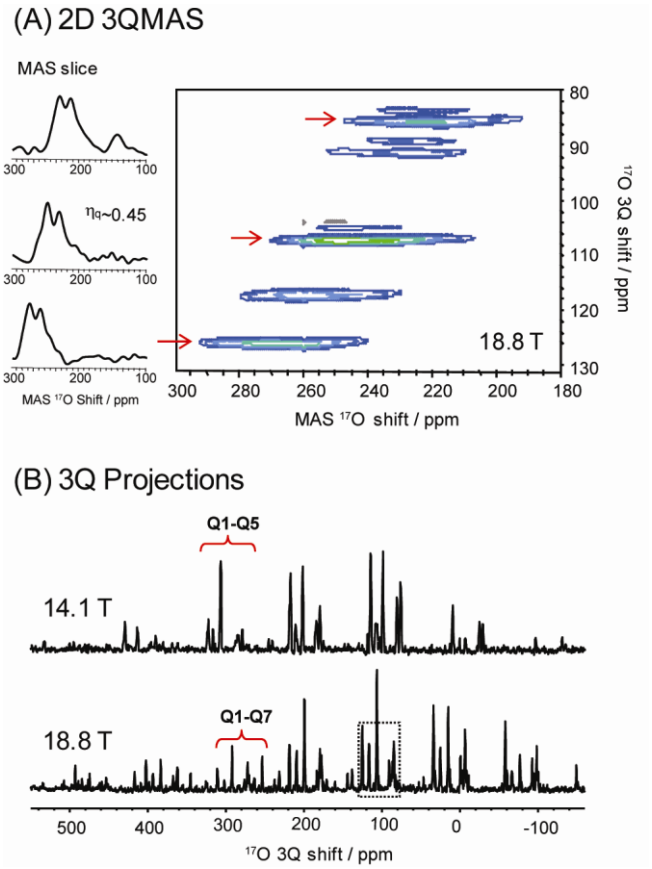

Figure 2. A Wong et al.

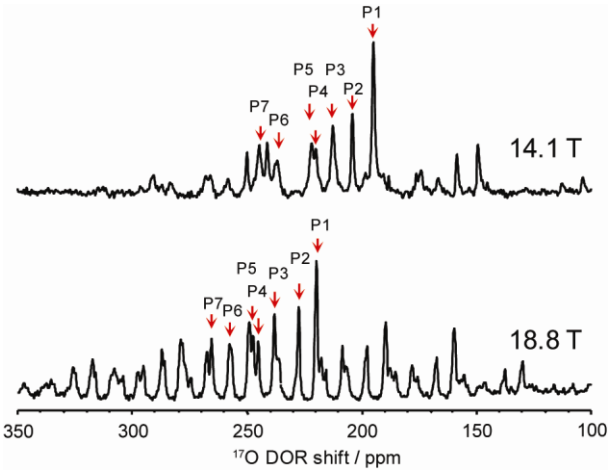

Figure 3. A Wong et al.

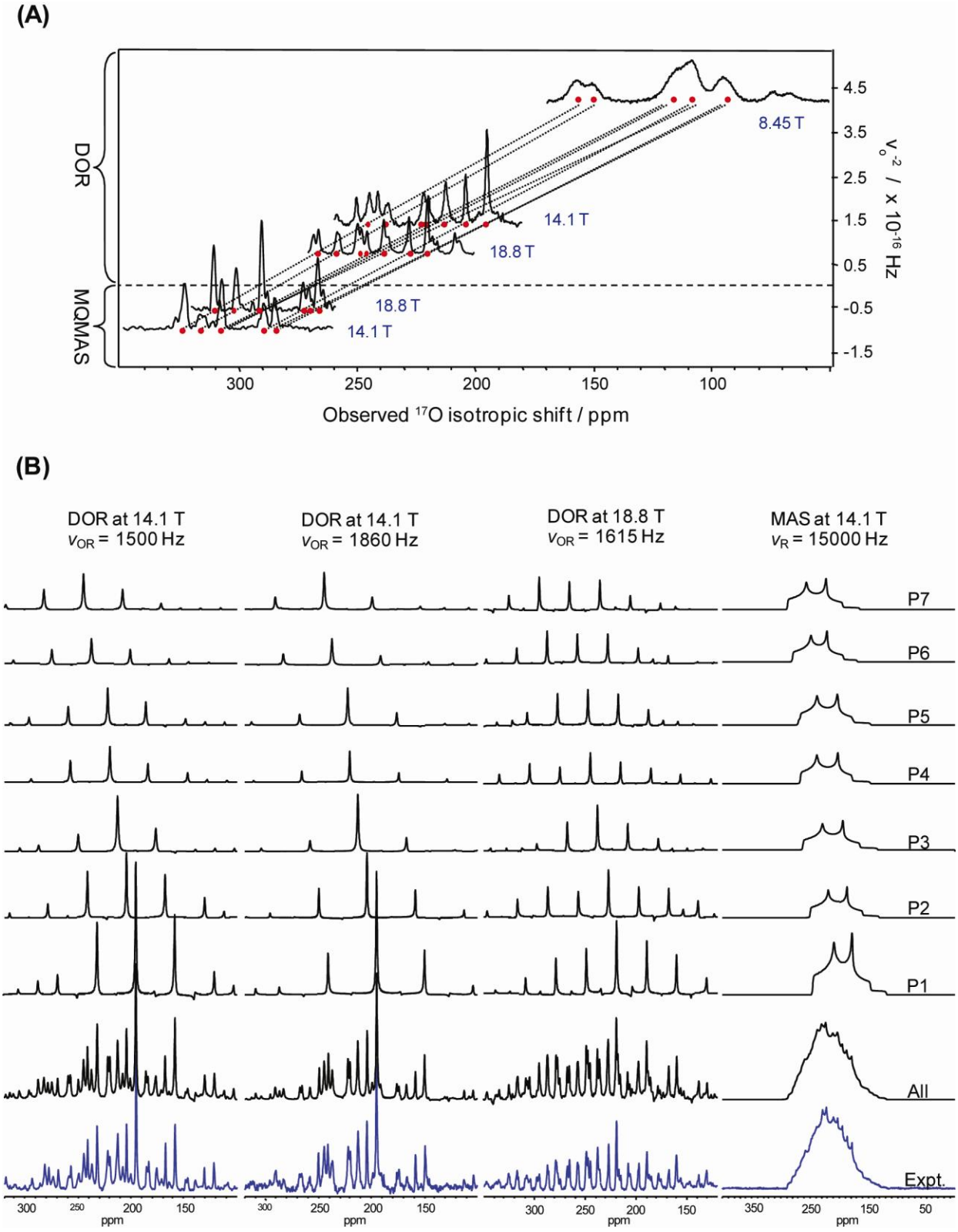

Figure 4. A Wong et al.

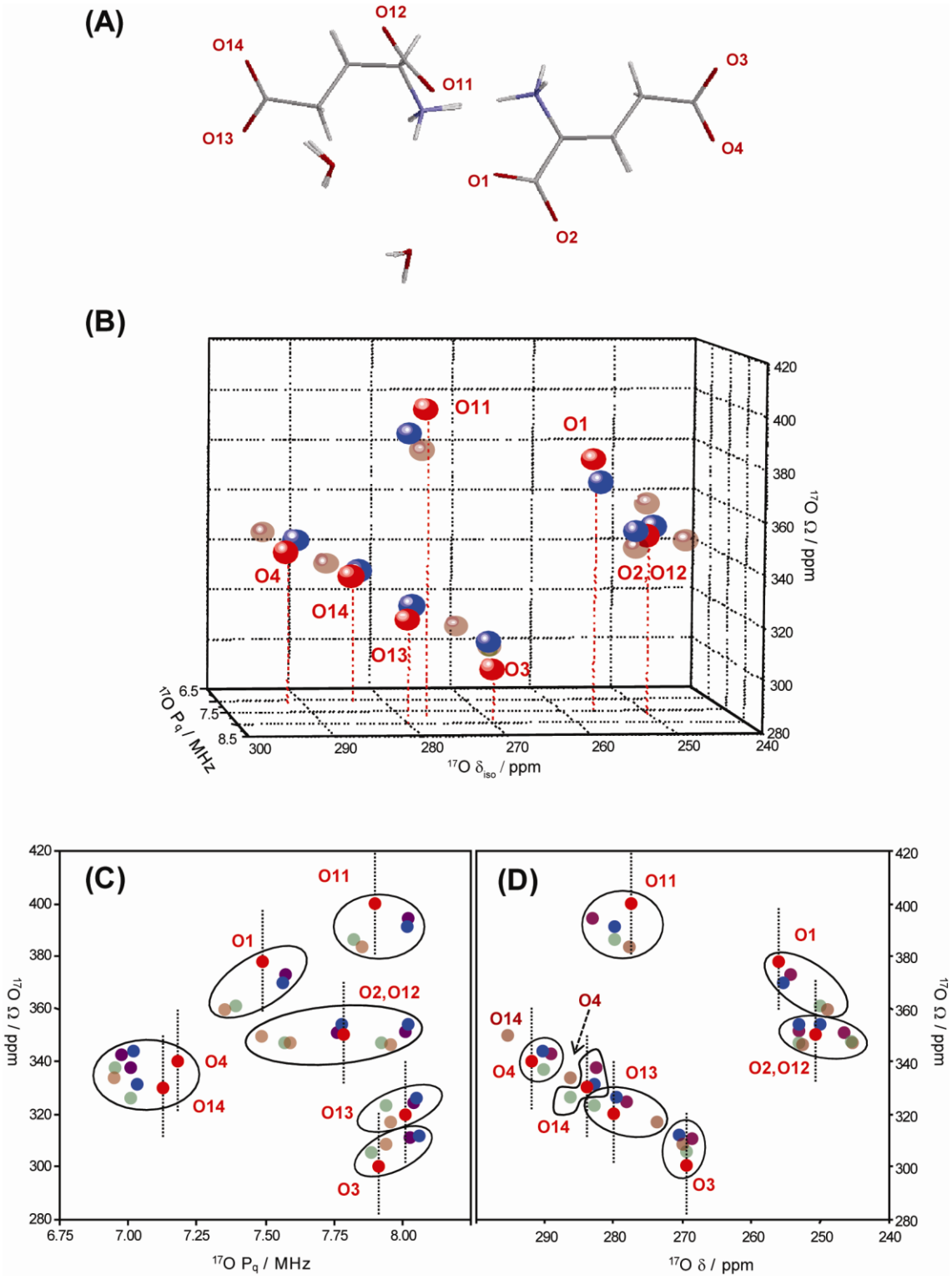

Figure 5. A Wong et al.

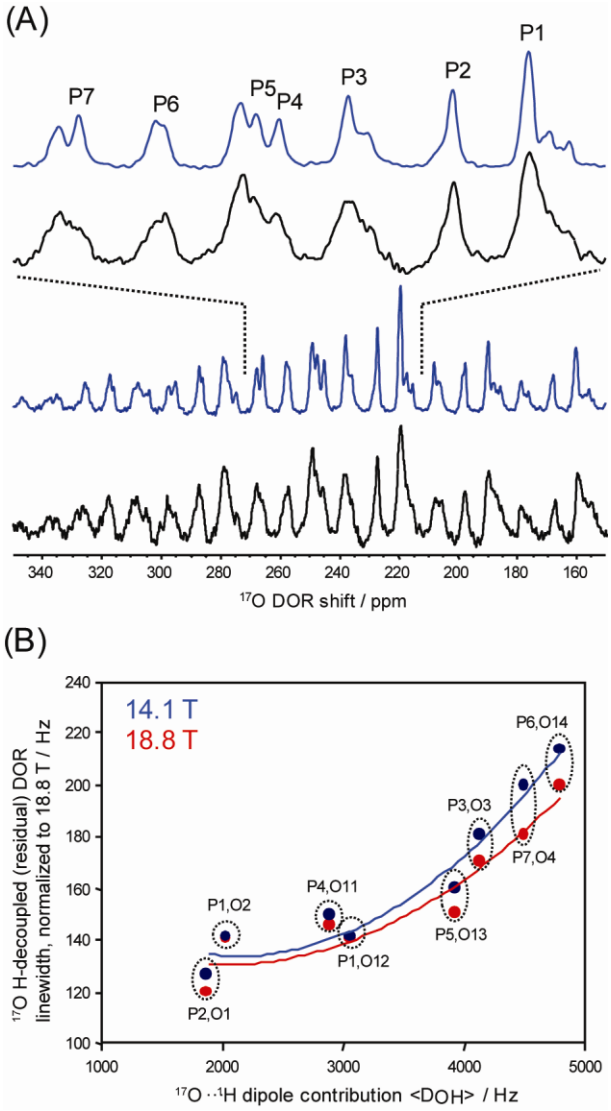

Figure 6. A Wong et al.

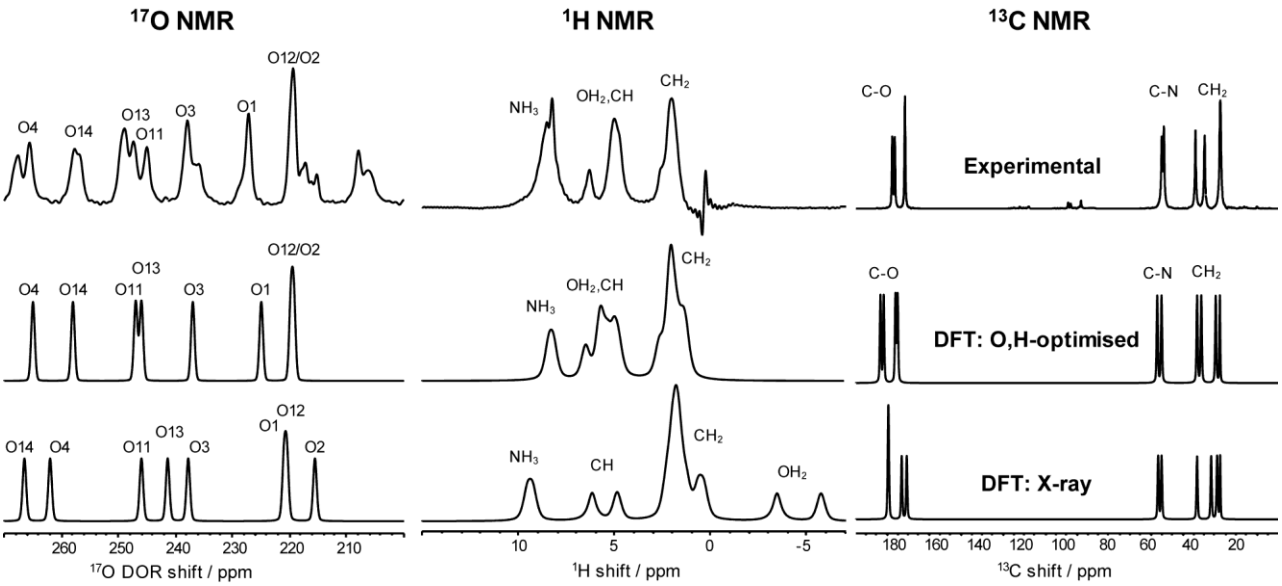

Figure 7. A Wong et al.

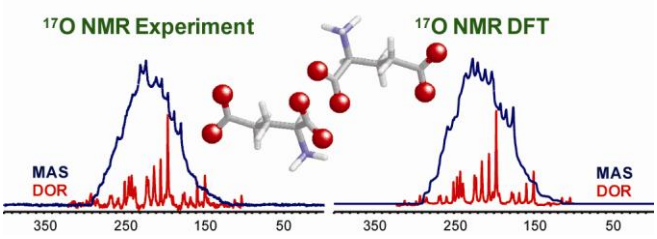

A comprehensive ^{17}O solid state NMR methodology that combines high resolution techniques and DFT calculations is demonstrated to develop ^{17}O approach for NMR crystallography.

TOC: A Wong et al.